

Squeezing electrons out of 6s² lone-pairs in perovskite-type oxides

Chun-Hai Wang,^{a,†} Paula Kayser,^{a,†} Brendan J. Kennedy,^a Helen E. Maynard-Casely,^b Qinfen Gu^c, and Chris D. Ling^{*a}

Having identified a set of conditions that predispose a solid-state ionic compound to a pressure-induced valence transition, we investigated a series of Bi(III) perovskite oxides. We found such a transition below 10 GPa in every case, including one that we synthesised for the first time (double perovskite-type Ba₂BiOsO₆).

While all ionic compounds have some degree of covalent bonding character, in solid-state chemistry it is convenient to treat them as collections of ions with well-defined formal oxidation states. Quantitative empirical concepts such as effective ionic radii (IR)¹ and bond valence sum (BVS)² are usually sufficient to understand the “crystal chemical” relationships among composition, structure and physical properties. These concepts predict that IR will decrease as electrons are removed from a shell (i.e., as the atom is oxidised): e.g., in 6-fold coordination, IR(Ir³⁺) = 0.68 vs. IR(Ir⁵⁺) = 0.57 Å (16% decrease). The change will be more pronounced when a shell is completely emptied: e.g., IR(Bi³⁺) = 1.03 vs. IR(Bi⁵⁺) = 0.76 Å (26% decrease). It will also be more pronounced when a so-called “valence skipping” element is involved, such as Bi or Pb. These encourage 2-electron transfers because the 6s² (Pb²⁺, Bi³⁺) and 6s⁰ (Pb⁴⁺, Bi⁵⁺) states are stable while the intermediate 6s¹ (Pb³⁺, Bi⁴⁺) states are not. When an ionic solid contains a suitable combination of ions, a net decrease in volume could, therefore, be achieved by an internal valence transfer: e.g., Bi³⁺Ir⁵⁺ → Bi⁵⁺Ir³⁺ would lead to a net contraction of an ionic lattice containing both elements. The thermodynamic favourability of such a process will be subject to external factors such as temperature and pressure. We recently discovered^{3,4} that this exact process takes place in the 12L-type perovskite Ba₄BiIr₃O₁₂,⁵ at ~5 GPa; the 6H-type perovskite Ba₃BiIr₂O₉,⁶ at ~6 GPa; and an analogous process involving the Ru⁵⁺/Ru³⁺ couple in the 6H-type perovskite Ba₃BiRu₂O₉,⁷ at ~9 GPa. We observed 1-2% volume collapses at these pressures by synchrotron X-ray powder diffraction for all three compounds, and by neutron powder diffraction for Ba₃BiIr₂O₉, with the latter experiment providing sufficiently precise Rietveld-refined Bi–O and Ir–O bond lengths to calculate BVS confirming the valence transition.³ A follow-up X-ray absorption spectroscopy experiment showed abrupt Bi, Ir and Ru edge shifts at the same pressures, also consistent with the valence transitions.⁴ The transitions were first-order and observed at the same pressures for all temperatures from 2–300 K, indicating that pressure is the dominant parameter, and proving that they are not directly related to the unusual temperature-driven magneto-elastic transitions exhibited by the same compounds.^{5, 8-10} The space-groups of all three compounds remained unchanged through the transitions.

Despite the conceptually straightforward explanation for such pressure-driven valence-state transitions, they are extremely rare in the literature. We are aware of only two directly analogous cases. The first case is the perovskite FeTiO₃, which undergoes a gradual transition Fe²⁺Ti⁴⁺O₃ → Fe³⁺Ti³⁺O₃ over the range 2–4 GPa.¹¹ The second, more recently reported, case is the quadruple perovskite LaCu₃Fe₄O₁₂, which at ~3.5 GPa¹² undergoes a first-order volume collapse accompanied by the internal charge transfer LaCu³⁺₃Fe³⁺₄O₁₂ → LaCu²⁺₃Fe^{3.75+}₄O₁₂. The same transition takes place on warming through 393 K,¹³ and the isostructural quadruple perovskites BiCu₃Fe₄O₁₂¹⁴ and SrCu₃Fe₄O₁₂¹⁵ undergo analogous transitions at 428 K at 210 K respectively – i.e., they undergo negative thermal expansion (NTE) because the effect of temperature on the stability of the valence states is contrary to its underlying thermodynamic effect on packing efficiency. We saw no such temperature-driven transition in Ba₄BiIr₃O₁₂,⁵ Ba₃BiIr₂O₉,⁶ or Ba₃BiRu₂O₉.⁷ Ostensibly similar temperature- and pressure-induced transitions have been observed in some oxides where the large “valence skipping” ion is located in a perovskite A-site, rather than a B-site as in the previous examples. However, the mechanism here is different: the melting of a charge-glass of disproportionated 6s²/6s⁰ ions into a purely 6s² state. This means that the high-pressure phase actually contains ions with a *larger* mean IR, defying the simple explanation used for the previous examples. The two distinct cases are the transitions (Bi³⁺_{0.5}Bi⁵⁺_{0.5})Ni²⁺O₃ → Bi³⁺Ni³⁺O₃ at ~3.5 GPa¹⁶ (which can be manipulated by La-doping for Bi¹⁷ and Fe-doping for Ni¹⁸), and (Pb²⁺_{0.5}Pb⁴⁺_{0.5})Cr³⁺O₃ → Pb²⁺Cr⁴⁺O₃ at ~2.4 GPa.¹⁹ They have been put forward as potentially tunable giant NTE materials (given that, again, the low-temperature phase has the larger volume). Finally, note that charge-ordering transitions, such as the Verwey transition in Fe₃O₄,^{20, 21} could be considered as special cases in which both ions are of the same element. The rarity of these transitions suggests that a compound’s electronic state must be particularly finely balanced for pressure and/or temperature to change its ground state in this way. In the work reported here, we set out to find more examples. We began by searching structural databases for oxides containing a cation with a 6s² (Tl⁺, Pb²⁺, Bi³⁺) or 5s² (Sn²⁺, Sb³⁺, Te⁴⁺) electron lone-pair at ambient pressure, in addition to a transition metal in an oxidation state lower than its highest stable state. The candidates we identified all contained Bi³⁺. These were the double-perovskite Ba₂BiIrO₆⁶ (Figure 1a) and the 8H perovskite Ba₂BiRuO₆²² (Figure 1b). We also hypothesised the existence of an additional phase, Ba₂BiOsO₆, which (as described below) we found to have the double perovskite structure of the Ir analogue. Every other

potential candidate was found, on closer inspection, to already be in the desired high-pressure phase at ambient pressure.

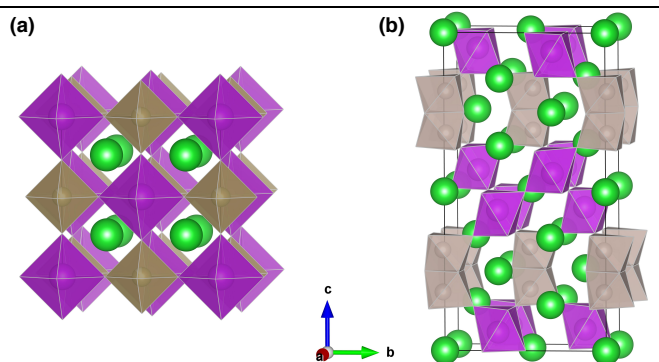


Figure 1. Structures of (a) double-perovskite Ba_2BilrO_6 (space group $Fm-3m$, isostructural with Ba_2BiOsO_6) and (b) 8H-perovskite Ba_2BiRuO_6 (space group $Cmcm$). Ba atoms are green, BiO_6 octahedra are purple, IrO_6 octahedra are gold and Ru_2O_9 face-sharing octahedral dimers are silver.

Polycrystalline (powder) samples of Ba_2BiRuO_6 ²² and Ba_2BilrO_6 ²³ were synthesized as described previously. Ba_2BiOsO_6 was prepared *via* solid-state chemistry in an evacuated sealed quartz tube. Stoichiometric amounts of BaO_2 (Aldrich 3N), Bi_2O_3 (Aithaca 4N) and Os (Aithaca 4N) (10% excess) were finely mixed as an acetone slurry in an agate mortar and heated at 850°C for 48 h. A second annealing at 850°C for 12 h in air was applied to eliminate the unreacted Os metal. Due to the possibility of producing toxic OsO_4 gas, the entire synthesis was carried out in a fumehood with appropriate PPE. Reaction progress was followed by X-ray powder diffraction (XRD), using a PANalytical X'Pert PRO in Bragg-Brentano reflection geometry with non-monochromated Cu K_α radiation ($\lambda = 1.5418 \text{ \AA}$) equipped with a PIXcel solid-state detector.

XRD data for Ba_2BiOsO_6 revealed it to be a double-perovskite isostructural with the high-temperature $Fm-3m$ (#225) form of Ba_2BilrO_6 ⁶ at room temperature. Figure 2 shows a Rietveld fit to at room temperature and pressure, with the final refined parameters in Table 1. A crystallographic information file (CIF) is available as Electronic Supplementary Information (ESI). Structure refinements against the XRD data were carried out using the Rietveld method²⁴ as implemented in the FULLPROF program²⁵. No regions were excluded in the refinement but a small (~2%) Bi_2O_3 impurity was modelled. The following parameters were refined: scale factor, zero-point error, background coefficients, peak shape (pseudo-Voigt), lattice parameters, atomic coordinates and occupancies. Note that the Bi and Os sites refined to their expected stoichiometric occupancies and bond valence sums (BVS)² within error.

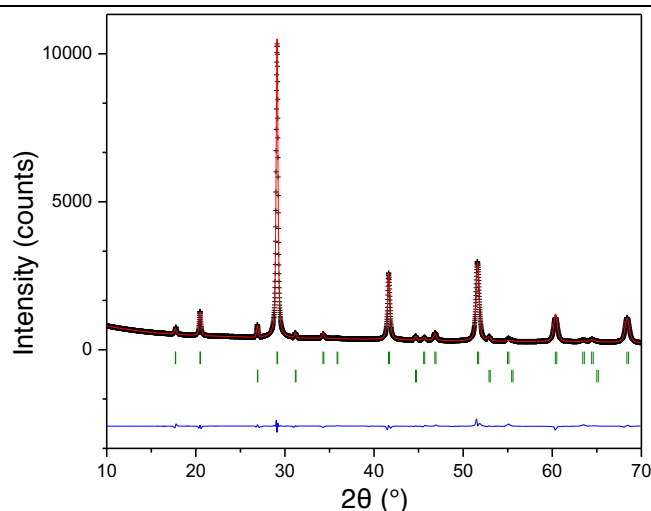


Figure 2. Observed (crosses), calculated (red line) and difference (blue line) profiles for the final Rietveld-refinements against XRD (Cu K_α) data for Ba_2BiOsO_6 . The vertical markers show the positions of the Bragg reflections for the main phase (upper row) and a minor Bi_2O_3 impurity (lower row).

High-pressure (HP) synchrotron XRD (S-XRD) data for all three samples were collected in a diamond-anvil cell (DAC) on the PD beamline of the Australian Synchrotron, and HP neutron powder diffraction (NPD) data for Ba_2BiRuO_6 were collected in a Paris-Edinburgh (P-E) press on the Wombat²⁶ diffractometer at ANSTO's OPAL reactor. Details of both HP experiments are available in the ESI file. Rietveld-refinements were carried out in the programs GSAS²⁷ with the EXPGUI²⁸ front-end (S-XRD) and TOPAS Academic²⁹ (NPD). The relatively high background and low counting statistics of the HP data meant that only unit cell parameters could be reliably refined, with other structural parameters fixed at the ambient pressure values. Further details and example fits are available in the ESI file.

Figure 3 shows reduced unit cell volumes of Ba_2BiRuO_6 , Ba_2BilrO_6 , and Ba_2BiOsO_6 vs. pressure, from Rietveld-refinement against HP S-XRD/NPD data. All three compounds undergo first-order volume collapses. As for $Ba_3Bilr_2O_9$, $Ba_3BiRu_2O_9$, and $Ba_4Bilr_3O_{12}$,³ there was no detectable change in space-group symmetry through the transitions. Note that the straight-line fits to the low- and high-pressure regions in Figures 3 and 4 are simply guides to the eye, because we had insufficient data points (especially in the high-pressure region) for a physically meaningful fit to an equation of states.

Table 1. Structural data for Ba_2BiOsO_6 , from Rietveld-refinement against XRD data at ambient pressure and 298 K. Space group $Fm-3m$ (#225): $a = 8.6704(2) \text{ \AA}$; $V = 651.81(3) \text{ \AA}^3$. Reliability factors: $R_p = 1.71\%$, $R_{wp} = 2.97\%$, $R_{exp} = 4.40\%$.

	$x(a)$	$y(b)$	$z(c)$	Occ.	BVS
Ba	$\frac{1}{4}$	$\frac{1}{4}$	$\frac{1}{4}$	1.00	1.44
Bi	0	0	0	1.2(2)	3.09
Os	$\frac{1}{2}$	$\frac{1}{2}$	$\frac{1}{2}$	0.8(1)	4.97
O	0.269(1)	0	0	1.00	2.00
Bi–O (Å)	2.339(9)				
Os–O (Å)	1.996(9)				

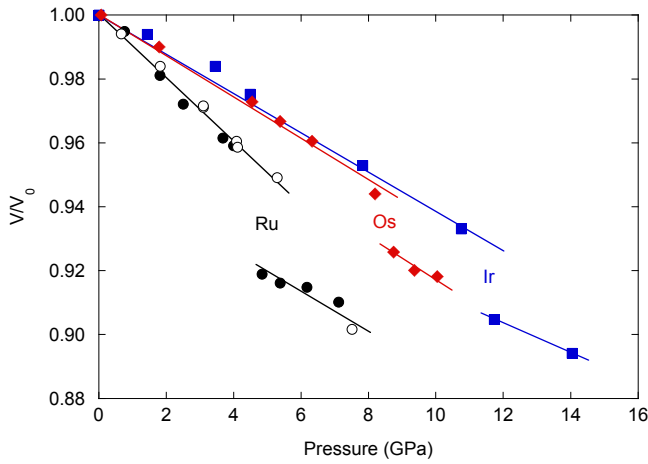


Figure 3. Reduced unit cell volumes for Ba_2BiRuO_6 (black circles) Ba_2BiIrO_6 (blue squares) and Ba_2BiOsO_6 (red diamonds) under pressure, from Rietveld-refinements against S-XRD (closed symbols) and NPD (open symbols) data. Errors bars are smaller than symbols; lines are guides to the eye.

The magnitudes of the volume collapses in Ba_2BiIrO_6 and Ba_2BiOsO_6 at 10 and 8 GPa respectively are consistent with expectations for $Bi \rightarrow M$ electron transfer. From the BVS formula, the ideal metal–oxygen bond lengths in regular BiO_6 and MO_6 octahedra are: $Bi^{3+} = 2.35 \text{ \AA}$; $Bi^{5+} = 2.13 \text{ \AA}$; $Ir^{3+} = 2.17 \text{ \AA}$; $Ir^{5+} = 1.98 \text{ \AA}$; $Os^{3+} = 2.07 \text{ \AA}$; $Os^{5+} = 1.88 \text{ \AA}$. The reaction $Ba_2Bi^{3+}Ir^{5+}O_6 \rightarrow Ba_2Bi^{5+}Ir^{3+}O_6$ should therefore give a linear reduction of $(2.13+2.17)/(2.35+1.98) = 0.993$, and or a volume reduction of $0.993^3 = 0.979$, or 2.1%. The calculation for the Os phase gives the same result, i.e., an expected 2.1% volume reduction, consistent with experimental observations shown in Figure 3. The contractions are isotropic, as expected from their structures. On top of the clear chemical analogy to our previous work on $Ba_3BiIr_2O_9$, $Ba_3BiRu_2O_9$, and $Ba_4BiIr_3O_{12}$, for which the valence transfer was independently confirmed by high-pressure NPD³ and XAS⁴ data, there can be little doubt as to the cause of these transitions in Ba_2BiIrO_6 and Ba_2BiOsO_6 .

We observed an even bigger volume collapse than expected (4%) in the 8H perovskite Ba_2BiRuO_6 , which also takes place at the lowest pressure (4 GPa). The transition is highly anisotropic (Figure 4), occurring predominantly along the c axis. Examining its 8H-type structure (Figure 1a), we see that unlike in the double-perovskites, the BiO_6 and RuO_6 octahedra do not have complete freedom to expand and contract independently: they must have approximately the same sized triangular faces in the ab -plane. This means that in the high-volume (ambient pressure) phase, the $Bi^{3+}O_6$ octahedra are constrained in that plane, and therefore extended along the c axis. This situation both destabilises the ambient-pressure phase, reducing the transition pressure; and causes the transition to be dominated by the c -axis contraction. A further particularity of Ba_2BiRuO_6 is the presence of double-layers of BiO_6 octahedra, which shows that $Bi-O-M$ linkages do not need to be strictly alternating for pressure-induced inter-site valence transfer.

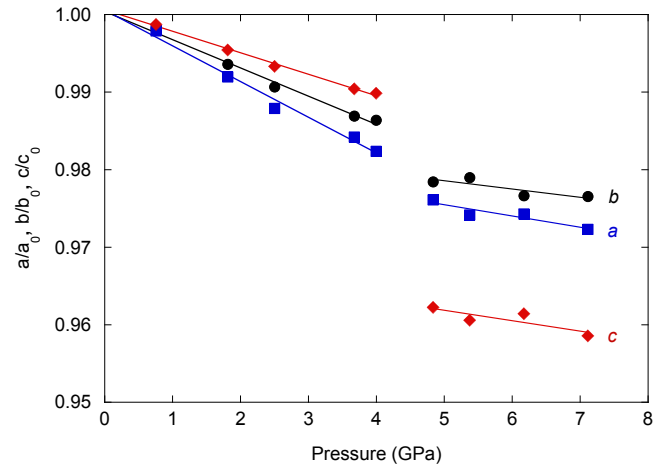


Figure 4. Reduced unit cell parameters for Ba_2BiRuO_6 under pressure, from Rietveld-refinements against S-XRD data. Errors bars are smaller than symbols; lines are guides to the eye.

A striking implication of the work presented here is that pressure-induced inter-site valence transitions may be far more common than previously thought. It seems likely that the paucity of reports is at least partly due to the inherent difficulties of high-pressure diffraction experiments. Such experiments are rarely done without the well-founded expectation of a positive outcome and a scientifically important result. With eight distinct known cases (including the three in this work), these expectations can now be higher.

The cases identified so far show clear patterns. In terms of composition, the fact that the majority exploit the large volume difference between Bi^{3+} and Bi^{5+} (26% reduction in IR) suggests that compounds with such “valence skipping” elements are the best candidates. The most obvious are Tl^+ and Pb^{2+} , which are isoelectronic with Bi^{3+} and show even larger IR reductions on losing the $6s^2$ lone-pair (41% and 35% respectively), and the $5s^2$ analogues Sb^{3+} and Te^{4+} (21% and 42% respectively; note that Sn^{2+} oxides are seldom observed). The larger the change, the more likely the transition, and the lower the pressure at which it should occur. The challenge is to find candidates that are not already in the “high-pressure” form at ambient pressure. In terms of structure, all cases thus far feature the large ion in a perovskite B -site, suggesting that continuous $M-O-M$ linkages through corner-sharing polyhedra are necessary, or at least helpful. Such linkages (a) facilitate electron transfer and (b) allow the structures to absorb a change in the relative volumes of constituent ions without a change in space-group symmetry (another feature of all cases thus far), lowering the activation barrier to the transition.

In terms of applications, while there has been significant interest in temperature-driven valence transitions, heightened by the possibility of tuning the NTE effect to elicit zero thermal-expansion, we have no evidence for high-temperature NTE transitions to the low-volume phases in any of our Bi-based compounds. The pressure-driven equivalents are of more fundamental interest. We would particularly like to tune them to lower pressures, to more easily measure physical properties such as resistivity. One approach could be to “pre-stress” them with chemical pressure, as we demonstrated by

the controlled doping of Sr²⁺ (IR = 1.44 Å) for Ba²⁺ (IR = 1.60 Å) to suppress the temperature-induced magneto-elastic transitions in Ba₃BiIr₂O₉ and Ba₃BiRu₂O₉.¹⁰ Our *ab initio* (density functional theory) calculations of the electronic densities of states for Ba₃BiIr₂O₉ suggested that the low-volume (high-pressure) form should be metallic, in contrast to the insulating high-volume (ambient-pressure) form. However, we have been unable to test and explore this predicted insulator-to-metal transition, which is all the more intriguing since the subsequent report of an insulator-to-metal transition in conjunction with the pressure-induced valence transfer in PbCrO₃.¹⁹ Large pressure-induced resistivity changes close to ambient pressures raise the possibility of pressure sensing applications, as well as a new way to explore and manipulate the solid-state physics of finely-balanced ground states.

Conflicts of interest

There are no conflicts to declare.

Acknowledgements

CDL and BJK received support for this work from the Australian Research Council (DP150102863).

Notes and references

1. R. D. Shannon, *Acta Crystallogr. A*, 1976, **32**, 751-767.
2. N. E. Brese and M. O'Keeffe, *Acta Crystallogr. B*, 1991, **47**, 192-197.
3. Z. Huang, J. E. Auckett, P. E. R. Blanchard, B. J. Kennedy, W. Miiller, Q. Zhou, M. Avdeev, M. R. Johnson, M. Zbiri, G. Garbarino, W. G. Marshall, Q. Gu and C. D. Ling, *Angew. Chem. Int. Ed.*, 2014, **53**, 3414-3417.
4. P. E. R. Blanchard, K. W. Chapman, S. M. Heald, M. Zbiri, M. R. Johnson, B. J. Kennedy and C. D. Ling, *Inorg. Chem.*, 2016, **55**, 5649-5654.
5. W. Miiller, M. T. Dunstan, Z. Huang, Z. Mohamed, B. J. Kennedy, M. Avdeev and C. D. Ling, *Inorg. Chem.*, 2013, **52**, 12461-12467.
6. C. Ling, B. Kennedy, Q. Zhou, J. Spencer and M. Avdeev, *J. Solid State Chem.*, 2010, **183**, 2739-2739.
7. J. Darriet, R. Bontchev, C. Dussarat, F. Weill and B. Darriet, *Eur. J. Solid State Inorg. Chem.*, 1993, **30**, 273-286.
8. W. Miiller, M. Avdeev, Q. Zhou, B. J. Kennedy, N. Sharma, R. Kutteh, G. J. Kearley, S. Schmid, K. S. Knight, P. E. R. Blanchard and C. D. Ling, *J. Am. Chem. Soc.*, 2012, **134**, 3265-3270.
9. W. Miiller, M. Avdeev, Q. Zhou, A. J. Studer, B. J. Kennedy, G. J. Kearley and C. D. Ling, *Phys. Rev. B*, 2011, **84**, 220406(R).
10. Z. Huang, M. Avdeev, B. J. Kennedy, K. S. Knight, Q. Zhou and C. D. Ling, *J. Phys. Condens. Matter*, 2014, **26**, 276003.
11. T. Seda and G. R. Hearne, *J. Phys. Condens. Matter*, 2004, **16**, 2707-2718.
12. Y.-w. Long, T. Kawakami, W.-t. Chen, T. Saito, T. Watanuki, Y. Nakakura, Q.-q. Liu, C.-q. Jin and Y. Shimakawa, *Chem. Mater.*, 2012, **24**, 2235-2239.
13. Y. W. Long, N. Hayashi, T. Saito, M. Azuma, S. Muranaka and Y. Shimakawa, *Nature*, 2009, **458**, 60-U63.
14. Y. Long, T. Saito, T. Tohyama, K. Oka, M. Azuma and Y. Shimakawa, *Inorg. Chem.*, 2009, **48**, 8489-8492.
15. I. Yamada, K. Tsuchida, K. Ohgushi, N. Hayashi, J. Kim, N. Tsuji, R. Takahashi, M. Matsushita, N. Nishiyama, T. Inoue, T. Irifune, K. Kato, M. Takata and M. Takano, *Angew. Chem. Int. Ed.*, 2011, **50**, 6579-6582.
16. M. Azuma, S. Carlsson, J. Rodgers, M. G. Tucker, M. Tsujimoto, S. Ishiwata, S. Isoda, Y. Shimakawa, M. Takano and J. P. Attfield, *J. Am. Chem. Soc.*, 2007, **129**, 14433-14436.
17. M. Azuma, W. T. Chen, H. Seki, M. Czapski, S. Olga, K. Oka, M. Mizumaki, T. Watanuki, N. Ishimatsu, N. Kawamura, S. Ishiwata, M. G. Tucker, Y. Shimakawa and J. P. Attfield, *Nat. Commun.*, 2011, **2**.
18. M. Azuma, Y. Sakai, T. Nishikubo, M. Mizumaki, T. Watanuki, T. Mizokawa, K. Oka, H. Hojo and M. Naka, *Dalton Trans.*, 2018, **47**, 1371-1377.
19. R. Yu, H. Hojo, T. Watanuki, M. Mizumaki, T. Mizokawa, K. Oka, H. Kim, A. Machida, K. Sakaki, Y. Nakamura, A. Agui, D. Mori, Y. Inaguma, M. Schlipf, K. Z. Rushchanskii, M. Ležaić, M. Matsuda, J. Ma, S. Calder, M. Isobe, Y. Ikuhara and M. Azuma, *J. Am. Chem. Soc.*, 2015, **137**, 12719-12728.
20. E. J. Verwey, P. W. Haayman and F. C. Romeijn, *J. Chem. Phys.*, 1947, **15**, 181-187.
21. E. J. W. Verwey and P. W. Haayman, *Physica*, 1941, **8**, 979-987.
22. J. Darriet, R. Bontchev, C. Dussarat, F. Weill and B. Darriet, *Eur. J. Solid State Inorg. Chem.*, 1993, **30**, 287-296.
23. C. D. Ling, B. J. Kennedy, Q. Zhou, J. R. Spencer and M. Avdeev, *J. Solid State Chem.*, 2010, **183**, 727-735.
24. H. Rietveld, *J. Appl. Crystallogr.*, 1969, **2**, 65-71.
25. J. Rodríguez-Carvajal, *Physica B Condens. Matter*, 1993, **192**, 55-69.
26. A. J. Studer, M. E. Hagen and T. J. Noakes, *Physica B Condens. Matter*, 2006, **385-86**, 1013-1015.
27. A. C. Larson and R. B. Von Dreele, *Los Alamos National Laboratory Report LAUR 86-748*, 1994.
28. B. Toby, *J. Appl. Crystallogr.*, 2001, **34**, 210-213.
29. A. A. Coelho, J. S. O. Evans, I. R. Evans, A. Kern and S. Parsons, *Powder Diffraction*, 2011, **26**, S22.